Microwave Engineering
Ulm University

universität
uulm

A Full Tensorial Synthesis Method for Holographic-Based Leaky Wave Antennas

Thomas Frey, Maximilian Döring, Christian Waldschmidt, Tobias Chaloun

DOI: 10.1109/LAWP.2023.3329586

A Full Tensorial Synthesis Method for Holographic-Based Leaky Wave Antennas

Thomas Frey, *Graduate Student Member, IEEE,* Maximilian Döring, *Graduate Student Member, IEEE,* Christian Waldschmidt, *Fellow, IEEE,* and Tobias Chaloun, *Senior Member, IEEE*

***Abstract*—In this work, a novel approach to extract the surface impedance tensor of a pixel geometry within a squared unit cell is presented. The scalar impedance is utilized to create a nonlinear system of equations resulting in an eigenmode impedance tensor for an arbitrary pixel geometry. A 3D-tensor database is created in order to assign the analytical impedance tensors to a physical pixel geometry in a single step procedure. Based on the tensorial synthesis method, an anisotropic holographic-based high-gain leaky wave antenna is realized on a fused silica wafer for an operation frequency of 160 GHz. The far field measurements show a gain of 32 dBi, a polarization purity of 38 dB, and a side-lobe level of 28 dB at 160 GHz. The input reflection coefficient is below −10 dB, and a maximum gain of 35 dBi is achieved across the bandwidth from 140 GHz to 170 GHz.**

***Index Terms*—impedance tensor extraction, anisotropic metasurface, holographic antenna, metasurface antenna.**

I. Introduction

Holographic-based leaky wave antennas (HLWAs) are based on the interaction of a surface wave (SW) with a periodic modulated surface. This can be achieved by a modulated impedance surface (MIS) constituted by a dense periodic structure of sub-wavelength discontinuities. The TM-based MIS structure is placed on a grounded dielectric slab to suppress the fundamental TE_0 SW mode. The MIS provides a highly flexible control in terms of the amplitude and phase of the objective aperture field distribution [1]–[4].

In recently published contributions, the scalar MIS is used to assign the analytical impedance tensor to a physical pixel geometry [5]–[9]. However, no unambiguous link between the course of the scalar surface impedance and the anisotropic degree of a pixel geometry is possible. In [10] the phase progression of the anisotropic tensor components is used to realize the anisotropic degree of the analytical impedance tensor. This scalar methodology results in inaccuracies, since only the secondary diagonal of the tensor is taken into account, and the isotropic components are not considered.

In this contribution, a novel method to extract the impedance tensor of an arbitrary shaped pixel geometry by solving a nonlinear system of equations (NLSoE) is presented. A 3D-impedance tensor database is created in order to assign the analytical impedance tensor to a physical pixel geometry. This results in an unambiguous and even more accurate assignment of the anisotropic impedance tensor to a corresponding pixel geometry, compared to the scalar methods, and leads to a significant improvement of the polarization purity and the antenna gain. The HLWA prototype is realized on a fused silica wafer, encouraged by very high manufacturing accuracy concerning the wet etching process at frequencies above 140 GHz. Furthermore, fused silica has an exceptional smooth surface and extremely dimensional stability due to its very low coefficient of thermal expansion [11].

This work was supported by the German Research Foundation under Grant CH 2226/4-1. (Corresponding author: Frey)

The authors are with the Institute of Microwave Engineering, Ulm University, 89081 Ulm, Germany e-mail: thomas.frey@uni-ulm.de.

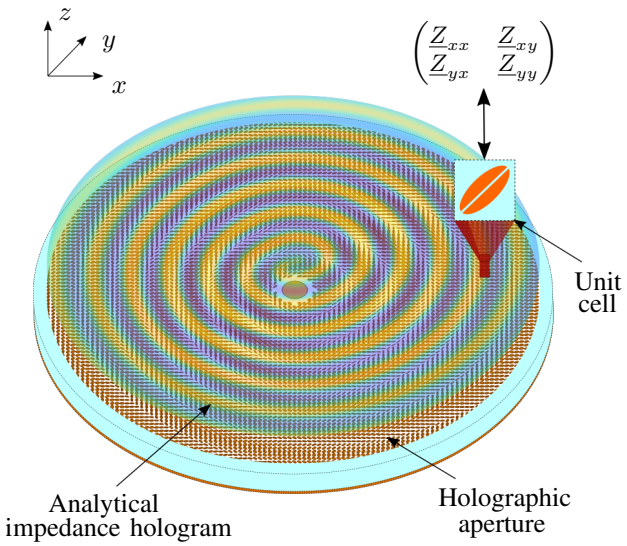

Fig. 1. Assignment of the analytical impedance tensor hologram to a holographic aperture consisting of a discrete set of unit cells and their corresponding pixel geometries. Conceptual drawing of the HLWA.

II. Synthesis for Holographic-Based Leaky Wave Antennas

For the purpose of a leaky wave (LW) radiation, an SW needs to be stimulated. The fundamental TM_0 SW mode is excited by a surface wave launcher (SWL), propagating rotationally symmetric on the antenna aperture [7]. Its transverse magnetic field distribution $\underline{\vec{H}}_{\mathrm{t}}|_{z=0^+}$ follows the Hankel function of the second kind and first order [2]. The SW interacts with an MIS which can be realized by a dense periodic structure of sub-wavelength discontinuities $\left(\approx \frac{\lambda_0}{10}\right)$, with λ_0 being the free space wavelength. The transverse electric field distribution $\underline{\vec{E}}_{\mathrm{t}}|_{z=0^+}$ and the surface current distribution $\underline{\vec{J}}_{\mathrm{surf}} = \vec{z} \times \underline{\vec{H}}_{\mathrm{t}}|_{z=0^+}$ on the antenna aperture at $z = 0^+$ are linked by the surface impedance tensor $\underline{\overleftrightarrow{Z}}$. This

relation is described by the space-dependent impenetrable impedance boundary condition (IIBC) [12], [13]

$$\begin{pmatrix} \underline{E}_{\mathrm{t},x}|_{z=0^+} \\ \underline{E}_{\mathrm{t},y}|_{z=0^+} \end{pmatrix} = \begin{pmatrix} \underline{Z}_{xx} & \underline{Z}_{xy} \\ \underline{Z}_{yx} & \underline{Z}_{yy} \end{pmatrix} \cdot \begin{pmatrix} \underline{J}_{\mathrm{surf},x} \\ \underline{J}_{\mathrm{surf},y} \end{pmatrix}, \tag{1}$$

where $\underline{Z}_{xx}$, $\underline{Z}_{yy}$ are the isotropic and $\underline{Z}_{xy}$, $\underline{Z}_{yx}$ are the anisotropic tensor components. The primary non-radiating transverse electric field portion of the $(0,0)$ and $(1,1)$ Floquet mode $\underline{E}_{\mathrm{t},(0,0)}$ and $\underline{E}_{\mathrm{t},(1,1)}$ has to be subtracted from the IIBC (1) to obtain the impedance tensor definition

$$\overleftrightarrow{\underline{Z}} \begin{pmatrix} \cos(\phi) \\ \sin(\phi) \end{pmatrix} = \underline{Z}_{\mathrm{avg}} \begin{pmatrix} \cos(\phi) \\ \sin(\phi) \end{pmatrix} + 2 \cdot \mathrm{Im}\left\{ \frac{\vec{\underline{E}}_{\mathrm{obj}}}{\underline{J}_{\mathrm{surf}}} \right\}, \tag{2}$$

depending on the average impedance $\underline{Z}_{\mathrm{avg}}$, the desired objective field $\vec{\underline{E}}_{\mathrm{obj}}$ and the SW surface current distribution [1], [2], [14]. The TM- and TE-components of the impedance tensor can be preserved by projecting (2) along the x- and y-direction. The spatial decay of the impedance tensor hologram in the x-y-plane is assumed by the space-dependent modulation indices M_x and M_y [4]. The result of the hologram synthesis is a holographic aperture consisting of analytical impedance tensors (see Fig. 1). That creates the object wave through the IIBC, whose radiating its main beam under (ϑ_0, ϕ_0) in the far field.

III. Modulated Impedance Surface Hologram

In order to realize the analytical MIS hologram by a discrete set of unit cells (UCs), a complex eigenmode problem of an infinite periodic UC structure is solved using HFSS [15]. A pixel is placed in the center of each UC. The pixel geometry is based on an elliptically shaped metal patch with an inclined slot (see Fig. 1). These pixel parameters are the pixel width w_{pxl} and the pixel orientation angle ϕ_{pxl}.

A. Scalar Impedance Hologram Synthesis

The complex eigenmode simulation offers only a scalar solution for the impenetrable surface impedance $\underline{Z}_{s,\mathrm{eig}}$ depending on the UC-referred incident angle ϕ_{inc}, the SW phase constant β_{SW}, the impedance of free space Z_{F0}, and k_0 the free-space wavenumber

$$\underline{Z}_{s,\mathrm{eig}}(\phi_{\mathrm{inc}}) = \mathrm{j} Z_{\mathrm{F0}} \sqrt{\left(\frac{\beta_{\mathrm{SW}}}{k_0}\right)^2 - 1}\,. \tag{3}$$

From the analytical model, an impedance tensor results for each UC. Consequently, for a meaningful assignment of the given impedance tensor to a pixel geometry, the calculation of its corresponding analytical scalar impedance is necessary. The angular-dependent scalar impedance $\underline{Z}_s(\phi_{\mathrm{inc}})$ for each UC can be obtained in (4) from [10]. A two-step procedure must be performed in order to assign the analytical impedance tensor to its corresponding anisotropic pixel geometry. In a first step, the pixel orientation angle ϕ_{pxl} must be computed for every UC by using the phase progression of the anisotropic tensor components. This results in a line vector containing all scalar impedance values over the pixel width. Subsequently, the minimum impedance error determines the pixel width w_{pxl} of the corresponding analytical scalar impedance [10].

B. Impedance Tensor Extraction

In order to determine the impedance tensor $\overleftrightarrow{\underline{Z}}_{\mathrm{eig}}$ of a pixel geometry, the eigenmode solution for the angular-dependent scalar surface impedance $\underline{Z}_{s,\mathrm{eig}}(\phi_{\mathrm{inc}})$ from (3) is used to create an NLSoE [16]. This requires the scalar impedance values at four different UCs incident angles ϕ_{inc} to solve the NLSoE for all the four unknowns. The NLSoE results in three solutions since $\overleftrightarrow{\underline{Z}} = -\overleftrightarrow{\underline{Z}}^{\mathrm{H}}$ is valid, whereas the fourth solution validates whether $\underline{Z}_{xy,\mathrm{eig}} = \underline{Z}_{yx,\mathrm{eig}}$ is fulfilled. The input values of ϕ_{inc} and the corresponding scalar impedance values $\underline{Z}_{s,\mathrm{eig}}(\phi_{\mathrm{inc}})$ have a significant influence on the impedance tensor solution of the NLSoE. For the incident angles $\phi_{\mathrm{inc},1} = 0°$ and $\phi_{\mathrm{inc},2} = 90°$, the NLSoE is considerably simplified. Furthermore, $\phi_{\mathrm{inc},3} = 45°$ and $\phi_{\mathrm{inc},4} = -45°$ are orthogonal to each other, resulting in a maximum difference between the corresponding scalar surface impedance values. For this reason, the four incident angles are chosen as follows:

$$\vec{\phi}_{\mathrm{inc}} = (\phi_{\mathrm{inc},1}, \phi_{\mathrm{inc},2}, \phi_{\mathrm{inc},3}, \phi_{\mathrm{inc},4})^{\mathrm{T}} = (0°, 90°, 45°, -45°)^{\mathrm{T}}.$$

The interested reader is referred to [10]. This reduces the complexity and yields to a very accurate solution for the eigenmode impedance tensor $\overleftrightarrow{\underline{Z}}_{\mathrm{eig}}$. The NLSoE has to be solved for every N pixel widths and all M pixel orientations, leading to a 3D-eigenmode tensor look-up table (LUT) $\overleftrightarrow{\underline{Z}}_{\mathrm{eig,LUT}}$ with $N \times M \times 4$ entries for the four tensor components. In Fig. 2 the eigenmode tensor components are shown for different pixel parameters w_{pxl} and

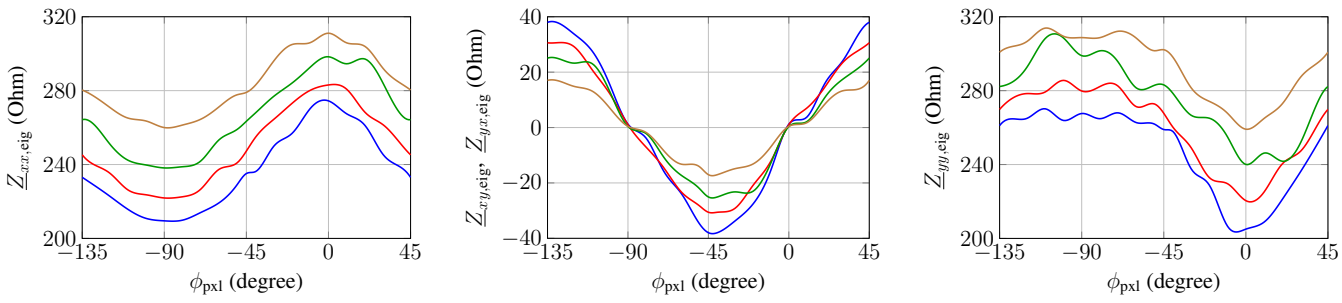

Fig. 2. Eigenmode impedance tensor for a slot-loaded elliptically shaped pixel calculated by the NLSoE for all pixel orientations $\phi_{\mathrm{pxl}} = [-135°, 45°]$ at 160 GHz and for the discrete pixel widths w_{pxl}: 90 µm (—), 120 µm (—), 150 µm (—), 180 µm (—), and a constant pixel length $l_{\mathrm{pxl}} = 180$ µm.

across the whole pixel orientation range. The pixel orientation angles $0°$ and $-90°$ yield an impedance tensor for which the anisotropic components vanish, since there is no electric field coupling into the TE-component. For $\phi_{\text{pxl}} = \pm 45°$ and $-135°$ a maximum TM/TE SW coupling occurs, leading to the maxima in the anisotropic impedance course.

C. Impedance Tensor Hologram Synthesis

In the scalar synthesis discussed in Sec. III-A, only the anisotropic tensor components are considered to determine the pixel orientation angle. But this assignment methodology is only an approximation and thus exhibits inaccuracies concerning the implementation of the anisotropic degree. Since a slot-loaded elliptical metal patch is used for the realization of the MIS, the SW surface current tends to flow along the elliptical shape and furthermore along the rotation direction of the inclined slot. The pixel orientation mainly influences the anisotropic tensor components $\underline{Z}_{xy}$, $\underline{Z}_{yx}$, and the pixel width primarily affects the main diagonal $\underline{Z}_{xx}$, $\underline{Z}_{yy}$ of the impedance tensor. Hence, all tensor components have an influence on the anisotropic degree. In order to realize the MIS even more accurate compared to the scalar synthesis, all tensor components must be involved for the assignment of the analytical impedance tensor to the pixel geometry.
The goal is to find the minimum impedance tensor error $\overleftrightarrow{e}$ between the analytical tensor and the eigenmode tensor LUT discussed in Sec. III-B to determine the physical pixel geometry parameters for each UC

$$\overleftrightarrow{e}\,(w_{\text{pxl},n}, \phi_{\text{pxl},m}) = \left| \overleftrightarrow{\underline{Z}}_{\text{eig,LUT}}\,(w_{\text{pxl},n}, \phi_{\text{pxl},m}) - \overleftrightarrow{\underline{Z}} \right|. \quad (4)$$

Subsequently, the ideal pixel geometry parameters are determined by the error tensor entry having the lowest impedance error across all four tensor components

$$(w_{\text{pxl}}, \phi_{\text{pxl}}) = \underset{w_{\text{pxl},n}, \phi_{\text{pxl},m}}{\arg\min} \left\{ \overleftrightarrow{e}\,(w_{\text{pxl},n}, \phi_{\text{pxl},m}) \right\}. \quad (5)$$

The extraction of the corresponding pixel geometry is now performed in a single step process. Thus, compared to the scalar method, an enhanced accuracy in the realization of the tensor is achieved. This tensorial hologram synthesis method is performed for every UC for the realization of the analytical impedance hologram as a holographic aperture (see Fig. 1).

IV. Design and Measurement

A. Design Process and Synthesis Comparison

Based on the synthesis process discussed in Sec. II, an anisotropic HLWA is designed on a fused silica wafer. In order to suppress higher order SW modes, the thickness of the glass wafer was chosen to $160\,\mu\text{m}$. The circular shaped glass wafer has an aperture diameter of $50.8\,\text{mm}$, and an SWL is placed in its center at $(x_{\text{f},1} = 0\,\text{mm}, y_{\text{f},1} = 0\,\text{mm})$. A coplanar waveguide (CPW) within the ground metallization is used to feed the SWL of the HLWA from the bottom side. A through-glass-via (TGV) connects the CPW line with the SWL on the upper side of the glass wafer. The CPW dimensions correspond to a characteristic impedance of $50\,\Omega$. The MIS

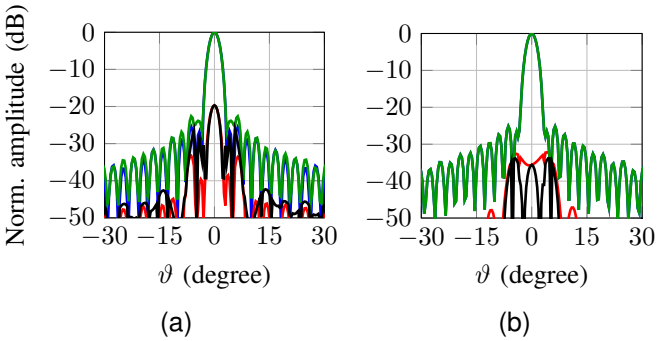

Fig. 3. Comparison of the simulated radiation patterns resulting from the IIBC hologram synthesis methods: (a) scalar synthesis and (b) tensor synthesis of the anisotropic HLWA on glass at 160 GHz. Co-pol (— $\phi_0 = 0°$, — $\phi_0 = 90°$) and cross-pol (— $\phi_0 = 0°$, — $\phi_0 = 90°$).

hologram consists of $45\,240$ squared UCs, and the UC size is set to $0.2\,\text{mm} \times 0.2\,\text{mm}$ to ensure a homogenize periodic structure. To realize the anisotropic impedance tensors, the pixel geometry is based on an elliptically shaped metal patch with an inclined slot. The proposed UC configuration provide an impedance variation from $\text{j}184\,\Omega$ to $\text{j}328\,\Omega$ leading to a maximum modulation index of $\max(M_{x,y}) = 0.28$ and an average impedance $\underline{Z}_{\text{avg}}$ of $\text{j}256\,\Omega$. For a meaningful comparison, both the scalar approach and the tensor method are used to create the holographic aperture. The designed HLWA is intended to radiate a right-hand circularly polarized (RHCP) pencil beam under the azimuth and elevation angles $(\vartheta_0 = 0°, \phi_0 = 0°)$ at $160\,\text{GHz}$. The co-polarization and cross-polarization of the simulated far field patterns resulting from the scalar approach (Sec. III-A) and the tensor method (Sec. III-C) are depicted in Figs. 3a and 3b. The radiation pattern based on the tensor hologram synthesis method provides a significant increase in the polarization purity of up to $15\,\text{dB}$. This results from the fact that in the calculation of the pixel orientation all tensor components are taken into account, leading to a more accurate implementation of the anisotropic degree. This is also reflected in the analytical antenna gain which increases by $2.4\,\text{dB}$ at $160\,\text{GHz}$. The side-lobe level (SLL) and $3\,\text{dB}$-beamwidth $\Delta\vartheta_{3\text{dB}}$ are almost identical to the scalar approach.

B. Realization and Measurement

The prototype of the anisotropic HLWA on glass, based on the tensor synthesis method (Sec. III-C), was fabricated on a fused silica wafer with a relative permittivity of $\varepsilon_r = 3.78$ and a loss tangent of $\tan\delta = 0.001$. The metallization of the periodic pixel structure and the ground plane consists of a $10\,\text{nm}$ thick chromium seed layer, on which a $350\,\text{nm}$ gold layer was sputtered. The individual pixel structures were realized by a conventional wet etching process with tolerances up to $\pm 2\,\mu\text{m}$. A probe tip in upside-down orientation is used to feed the antenna on glass from the bottom side. The similar measurement setup has been used as described in [7]. The realized prototype of the anisotropic HLWA on glass is depicted in Fig. 4a. The far field measurements are conducted using a robot-supported mm-wave antenna measurement setup [17], [18]. The co- and cross-polarization

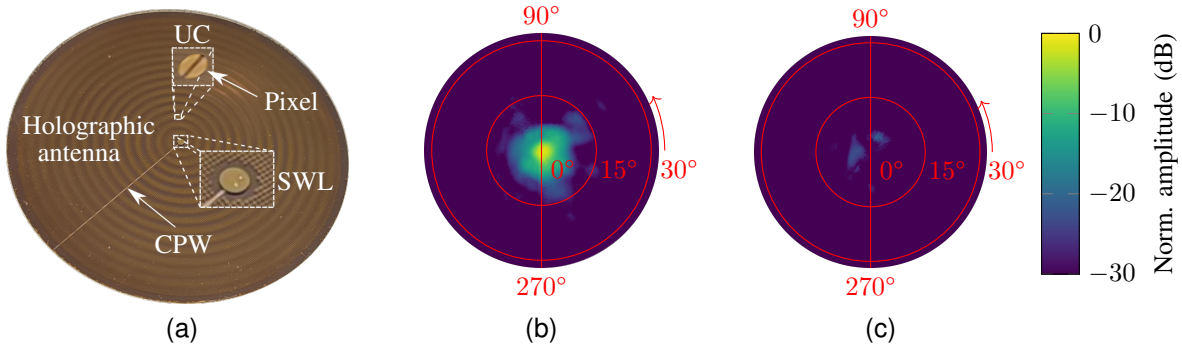

Fig. 4. Measured 3D-radiation patterns of the anisotropic HLWA on glass: (a) realized prototype, (b) co-pol, and (c) cross-pol at 160 GHz.

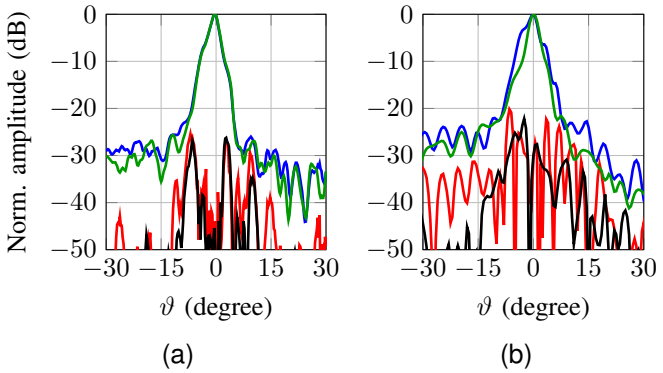

Fig. 5. Measured radiation patterns of the anisotropic HLWA on glass. In (a) co-pol (— $\phi_0 = 0°$, — $\phi_0 = 90°$) and cross-pol (— $\phi_0 = 0°$, — $\phi_0 = 90°$) at 160 GHz. In (b) co-pol (— $\phi_0 = 0°$), cross-pol (— $\phi_0 = 0°$) at 158 GHz and co-pol (— $\phi_0 = 0°$), cross-pol (— $\phi_0 = 0°$) at 164 GHz.

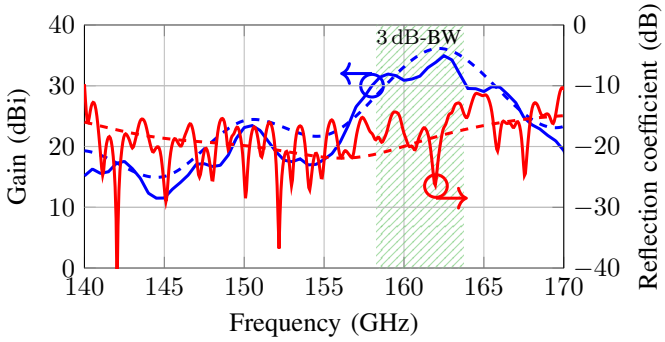

Fig. 6. Measured (solid line) and simulated (dashed line) antenna gain (—) and reflection coefficient (—) for the realized HLWA on glass vs. frequency from 140 GHz to 170 GHz.

components of the measured 3D-radiation patterns are shown in Figs. 4b and 4c for elevation angles up to ±30° and for all azimuth angles. The shape of the main beam, the SLL, and the polarization purity are very well-defined in all azimuth planes. In Fig. 5 the measured far field patterns of the HLWA are illustrated for an elevation angle range of ±30°. Fig. 5a shows the radiation pattern at the azimuth angles 0° and 90° for an operation frequency of 160 GHz. A minimum SLL of 28 dB and a polarization purity of 38 dB were measured at 160 GHz. The measured antenna gain equals 35 dBi, and the input reflection coefficient is below −10 dB

TABLE I
COMPARISON TABLE TO THE STATE-OF-THE-ART.

Lit.	Meas. gain (dBi)	f (GHz)	Size (λ_0^2)	SLL (dB)	Pol. purity (dB)	AE (%)
o. w.	32.0	160	448	28.0	38.0	28.3
[1]	20.0 (sim.)	13	43	15.0	16.0	18.5
[7]	24.7	150	306	15.0	16.7	7.6
[19]	20.0 (sim.)	300	50	17.0	15.0	15.9
[16]	21.8	10	115	16.0	19.6	10.4
[20]	26.0	9.5	113	31.0	20.0	30.0

across the wide frequency range from 140 GHz to 170 GHz, as depicted in Fig. 6. The stopband phenomenon is suppressed, since the impedance hologram is 180° out-of-phase w.r.t. its origin. This leads to a destructive interference of all SWs reflected at the UCs on the antenna aperture. The measurement results agree very well with the simulations. Furthermore, a measured 3 dB-bandwidth (3 dB-BW) regarding the antenna gain of 6 GHz from 158 GHz to 164 GHz can be determined from Fig. 6. The measured radiation patterns at 158 GHz and 164 GHz are shown in Fig. 5b for the azimuth angle 0°. The computed directivity based on the measured 3D-radiation pattern is 35.7 dBi, corresponding in a radiation efficiency of at least 83 % within the entire bandwidth of 30 GHz. A comparison with other state-of-the-art HLWA synthesis methods, based on TM SW mode excitations, is listed in Table I. As can be seen, the presented tensor synthesis method achieves a significant improvement concerning gain, SLL, polarization purity and AE for HLWAs.

V. Conclusion

In this paper, a novel impedance tensor extraction method for an arbitrary pixel geometry within a squared unit cell is presented. The scalar surface impedance is used for this purpose to create a nonlinear system of equations, whose solution corresponds to the eigenmode impedance tensor. A 3D-tensor database is created to assign the analytical impedance tensor to a physical pixel geometry, which is even more accurate compared to the scalar approach. Based on the tensor synthesis, an anisotropic HLWA is realized on a fused silica wafer, operating at 160 GHz. The measured radiation patterns show a high maximum gain of 35 dBi, a polarization purity of 38 dB, and a side-lobe level of 28 dB.

ACKNOWLEDGMENT

This work was supported by the German Research Foundation under Grant CH 2226/4-1. The authors would like to thank to Norbert Ambrosius from LPKF Laser & Electronics AG for processing and machining the glass wafer to realize the holographic antenna prototype.

REFERENCES

[1] G. Minatti, F. Caminita, M. Casaletti, and S. Maci, "Spiral Leaky-Wave Antennas Based on Modulated Surface Impedance," *IEEE Transactions on Antennas and Propagation*, vol. 59, no. 12, pp. 4436–4444, Dec. 2011.

[2] G. Minatti, M. Faenzi, E. Martini, F. Caminita, P. D. Vita, D. González-Ovejero, M. Sabbadini, and S. Maci, "Modulated Metasurface Antennas for Space: Synthesis, Analysis and Realizations," *IEEE Transactions on Antennas and Propagation*, vol. 63, no. 4, pp. 1288–1300, Apr. 2015.

[3] G. Minatti, F. Caminita, E. Martini, and S. Maci, "Flat Optics for Leaky-Waves on Modulated Metasurfaces: Adiabatic Floquet-Wave Analysis," *IEEE Transactions on Antennas and Propagation*, vol. 64, no. 9, pp. 3896–3906, 2016.

[4] T. Frey, A. Dürr, C. Waldschmidt, and T. Chaloun, "Holographic Conical Beam Scanning Antenna for mm-Wave Radars Using Glass Technology," in *51st European Microwave Conference (EuMC)*, 2022, pp. 825–828.

[5] S. Pandi, C. A. Balanis, and C. R. Birtcher, "Design of scalar impedance holographic metasurfaces for antenna beam formation with desired polarization," *IEEE Transactions on Antennas and Propagation*, vol. 63, no. 7, pp. 3016–3024, 2015.

[6] M. Casaletti, M. Śmierzchalski, M. Ettorre, R. Sauleau, and N. Capet, "Polarized beams using scalar metasurfaces," *IEEE Transactions on Antennas and Propagation*, vol. 64, no. 8, pp. 3391–3400, 2016.

[7] T. Galler, T. Frey, C. Waldschmidt, and T. Chaloun, "High-Gain Millimeter-Wave Holographic Antenna in Package using Glass Technology," *IEEE Antennas and Wireless Propagation Letters*, pp. 2067–2071, 2020.

[8] M. Döring, T. Frey, C. Waldschmidt, and T. Chaloun, "High-Gain Holographic Multi-Feed Antenna," in *14th German Microwave Conference (GeMiC)*, 2022, pp. 01–04.

[9] T. Frey, M. Döring, N. Riese, C. Waldschmidt, and T. Chaloun, "Angle-Dependent Synthesis Method for Holographic Multi-Feed Antennas," *IEEE Open Journal of Antennas and Propagation*, vol. 4, pp. 392–407, 2023.

[10] T. Frey, M. Döring, C. Waldschmidt, and T. Chaloun, "Towards Holographic Antenna Systems for MIMO Radar and Communication Applications," in *16th European Conference on Antennas and Propagation (EuCAP)*, 2022, pp. 1–5.

[11] T. Chaloun, S. Brandl, N. Ambrosius, K. Kröhnert, H. Maune, and C. Waldschmidt, "RF Glass Technology Is Going Mainstream: Review and Future Applications," *IEEE Journal of Microwaves*, vol. 3, no. 2, pp. 783–799, 2023.

[12] E. Bleszynski, M. Bleszynski, and T. Jaroszewicz, "Surface-integral equations for electromagnetic scattering from impenetrable and penetrable sheets," *IEEE Antennas and Propagation Magazine*, vol. 35, no. 6, pp. 14–25, 1993.

[13] M. A. Francavilla, E. Martini, S. Maci, and G. Vecchi, "On the numerical simulation of metasurfaces with impedance boundary condition integral equations," *IEEE Transactions on Antennas and Propagation*, vol. 63, no. 5, pp. 2153–2161, 2015.

[14] A. Oliner and A. Hessel, "Guided waves on sinusoidally-modulated reactance surfaces," *IRE Transactions on Antennas and Propagation*, vol. 7, no. 5, pp. 201–208, 1959.

[15] HFSS version 19.2, Ansys Cooperation, Canonsburg, PA, USA, 2019.

[16] B. H. Fong, J. S. Colburn, J. J. Ottusch, J. L. Visher, and D. F. Sievenpiper, "Scalar and Tensor Holographic Artificial Impedance Surfaces," *IEEE Transactions on Antennas and Propagation*, vol. 58, no. 10, pp. 3212–3221, Oct. 2010.

[17] L. Boehm, F. Boegelsack, M. Hitzler, and C. Waldschmidt, "The Challenges of Measuring Integrated Antennas at Millimeter-Wave Frequencies [Measurements Corner]," *IEEE Antennas and Propagation Magazine*, vol. 59, no. 4, pp. 84–92, Aug. 2017.

[18] ——, "Enhancements in mm-wave antenna measurements: automatic alignment and achievable accuracy," *IET Microwaves, Antennas Propagation*, vol. 11, no. 12, pp. 1676–1680, 2017.

[19] D. González-Ovejero, C. Jung-Kubiak, M. Alonso-delPino, T. Reck, and G. Chattopadhyay, "Design, fabrication and testing of a modulated metasurface antenna at 300 GHz," in *11th European Conference on Antennas and Propagation (EUCAP)*, 2017, pp. 3416–3418.

[20] M. Teniou, H. Roussel, M. Serhir, N. Capet, G. Piau, and M. Casaletti, "Experimental Validation of Tensorial Metasurfaces for the Implementation of Radiating Aperture Field Distributions," *IEEE Transactions on Antennas and Propagation*, vol. 67, no. 7, pp. 4901–4906, 2019.